ChemComm

Accepted Manuscript

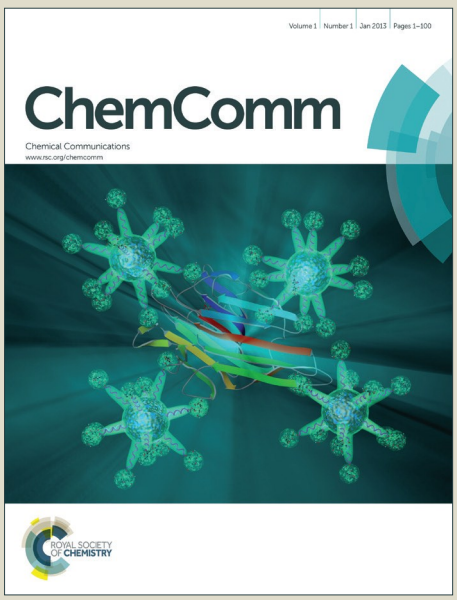

ROYAL SOCIETY OF CHEMISTRY

www.rsc.org/chemcomm

Table of Content

In-grown structure of oxides and CNT hybrid strongly favors the charge transfer at the interface leading to high electrochemical performance.

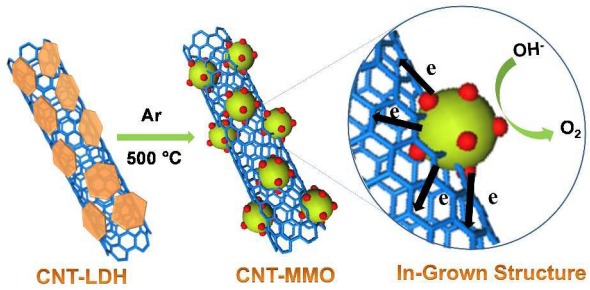

ChemComm

COMMUNICATION

In-Grown Structure of NiFe Mixed Metal Oxides and CNT Hybrid Catalyst for Oxygen Evolution Reaction

Received 00th October 2015,
Accepted 00th October 2015

DOI: 10.1039/x0xx00000x

www.rsc.org/

Yongmei Li[a], Haiyong He[a], Wei Fu[a], Chenzhong Mu[a], Xiu-Zhi Tang[b], Zheng Liu[a], Dongzhi Chi[c], Xiao Hu[a]*

This work reports an unqiue In-grown structure of NiFe/CNT hybrid catalyst. This structure creates larger interfacial area and strong interaction between NiFe catalyst and CNT, which could promote the charge transfer at the interface, and hence improve the conductivity. This leads to oustanding electrochemical performance for oxygen evolution reaction.

Oxygen evolution reaction (OER) is an electrochemical oxidation process to convert water into O_2, in which form energy is stored.[1, 2] It plays a very important role in applications of energy conversion and storage, e.g., water splitting and rechargeable metal air batteries.[3-5] Research for more efficient OER catalysts has received considerable attention in the field of energy related applications.

So far, RuO_2 and IrO_2 are reported to be the most active catalyst for OER process, but they are expensive and scarce.[6, 7] Transition metals such as Ni, Co, Mn, Sn, Ti, V hydroxides or oxides are studied as an alternative replacement.[8-11] Among them, Ni based catalyst, such as NiO[12, 13] and $Ni(OH)_2$[12, 14], has been intensively studied because of its high catalytic activity, stability and low cost. However, the poor electrical conductivity limits their electrochemical performance. In the recent years, Ni-Fe oxyhydroxide ($Ni_{1-x}Fe_xOOH$)[15-17] and NiFe layered double hydroxide (LDH)[18-21] is intensively studied for OER. Trotochaud et al. reported that, loading of Fe could not only improve the conductivity, but also modify the electronic structure of NiOOH making it highly reactive for electrochemical performance.[17] To further enhance the conductivity of NiFe based catalyst, electrically conducting materials such as Ni foam[11, 18], graphene[22-24], carbon nanotube (CNT)[25, 26], and carbon quantum dots[27] have been used to hybridize with NiFe LDH. Gong et al. reported that better OER activity and stability could be obtained from the hybrid material of NiFe LDH and CNT than that of commercial Ir catalyst.[25] However, the NiFe LDH is simply coupled with CNT through physical adsorption in their study.

In this study, we report an in-grown structure of NiFe mixed metal oxides (MMO) and CNT hybrid catalyst. This structure strongly favors the charge transfer process at the interface due to the increased interfacial area and strong interaction between MMO and CNT. With the efficient charge transfer process at the interface, the overall conductivity of the hybrid is significantly improved. As a result, this hybrid catalyst shows excellent OER performance with onset potential of 1.43 V vs. RHE and tafel slope of 45 eV/dec as well as excellent durability in alkaline solution.

Transmission electron microscopy (TEM) image shows that NiFe LDH nanoplates with diameter of ~3 nm are successfully deposited on CNT surface (Fig. 1A). The low magnification TEM image (Fig. S1A, ESI†) and the scanning electron microscopy (SEM) image (Fig. S2A, ESI†) of CNT-LDH show that this morphology is generally uniform. After calcination, the particle diameters are increased to 5-10 nm as shown in Fig. 1B. Comparing with Fig. 1A, the CNT-MMO catalyst exhibits an In-grown structure, i.e. some holes, marked with yellow line, can be clearly observed at the CNT wall and filled up with NiFe MMO nanoparticles (Fig. 1B). The low magnification TEM image (Fig. S1B, ESI†) and SEM image (Fig. S2B, ESI†) of CNT-MMO show that the MMO particles are uniformly distributed on CNT. In addition, the fibrous structure of CNT is not destroyed during the calcination process. The dark field image of CNT-MMO obtained through scanning transmission electron microscopy (STEM) is shown in Fig. 1C, and the overlapped image of elemental mapping at this position is shown in Fig. 1D (the elemental mapping of Ni, Fe, and O is shown in Fig. S3, ESI†). The STEM image evidence the intimately mixed NiFe MMO. Such intimate mixture of Ni and Fe could magnify the

[a] School of Materials Science and Engineering, Nanyang Technological University, Nanyang Avenue, Singapore 639798.
[b] School of Mechanical and Aerospace Engineering, Nanyang Technological University, Nanyang Avenue, Singapore 639798.
[c] Institute of Materials Research and Engineering (IMRE), 3 Research Link, Singapore 117602.
* Corresponding author: e-mail: asxhu@ntu.edu.sg; Fax: (65) 6790 9081; Tel: (65) 6790 4610.

† Electronic Supplementary Information (ESI) available: Synthesis of catalysts, Characterization, Electrochemical Measurement, SEM images, TEM images, STEM mapping, XRD, XPS, corrected polarization curves of CNT-MMO and CNT-LDH catalysts, Electrochemical performance data of reference work. See DOI: 10.1039/x0xx00000x

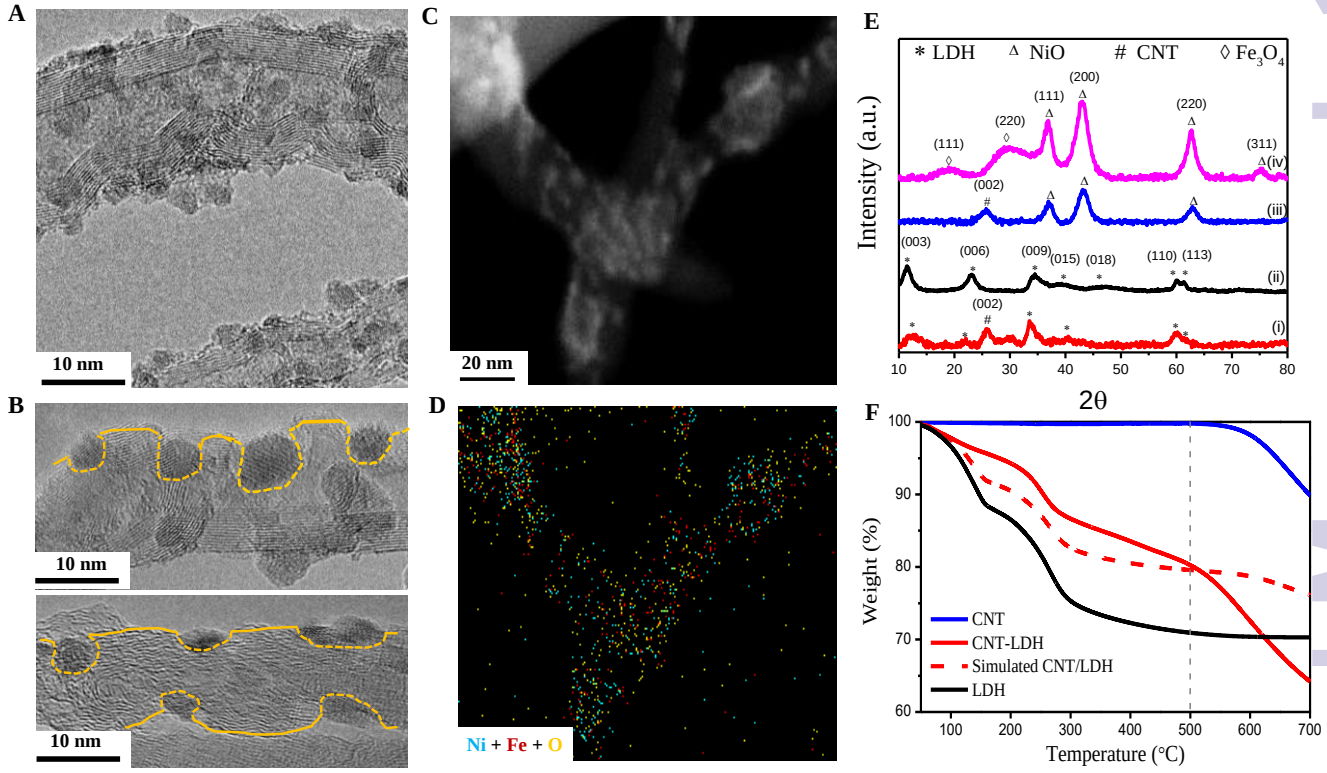

Fig. 1 (A) TEM image of CNT-LDH; (B) TEM image of CNT-MMO; (C) STEM dark field image of CNT-MMO; (D) The overlapped image of elemental mapping distribution, which shows the Ni, Fe, and O of CNT-MMO for the position corresponding to the image (C); (E) XRD spectra of i. CNT-LDH ii. NiFe LDH iii. CNT-MMO iv. Calcined NiFe LDH; (F) TGA curves of CNT, CNT-LDH, LDH, simulated CNT/LDH (the simulated weight loss curve for CNT/LDH is the sum of weight loss for 30 wt% CNT and 70 wt% LDH, which is the same ratio as in CNT-MMO catalyst).

role of Fe in the enhancement of electrochemical performance.[17]

To investigate the change of crystal structure, the x-ray diffraction (XRD) measurement was carried out. The XRD spectrum of CNT-LDH is shown in Fig. 1E-i. The CNT (002) peak is identified, and the other peaks are assigned to NiFe LDH, which is the same as those of pure NiFe LDH (Fig. 1E-ii). Fig. 1E-iii is the XRD spectrum of CNT-MMO catalyst. The CNT (002) peak and NiO peaks are clearly shown. We can conclude all LDH crystals are converted to oxide. It is interesting that the peak at 18.9° and 29.4° in Fig. 1E-iv belonging to iron oxide is not revealed in the XRD spectra of CNT-MMO.

In order to confirm the optimum calcination temperature, the thermo-gravimetric analysis (TGA) experiments were carried out (Fig. 1F). The weight loss of CNT from 550 °C is due to the removal of the functional groups.[28] Two stages of weight loss for LDH are corresponding to the dehydroxylation and decomposition process. CNT-LDH shows similar weight loss profile with that of simulated CNT/LDH before the intercept at 500 °C. And then, the CNT-LDH shows significantly weight loss which is attributed to the reaction between CNT and NiO, i.e. carbon reduction reaction. Therefore, we use 500 °C as the calcination temperature. If the temperature is above 500 °C, the reaction is too fast and very difficult to control.

To investigate the growth mechanism of the In-grown structure, time dependent experiments were carried out. With 0.5 hr calcination, LDH were converted into MMO as studied by the XRD spectrum in Fig. S4-i (ESI†), where NiO peaks are identified. However, the TEM images (Fig. S5A and Fig. S6A, ESI†) show the nanoparticles exist only on the CNT surface, and the in-grown structure cannot be observed. This is the case of physical adsorption. With increased calcination duration up to 3 hr, the TEM images (Fig. S5B and Fig. S6B, ESI†) show that the tubular structure of CNT is destroyed, and NiO particles grow larger. The increased particle size is also verified by the shaper XRD peak intensity of NiO (200) (Fig. S4-ii, ESI†), comparing with that of CNT-LDH-0.5 hr.

The XPS analysis of C 1s, Ni 2p3/2, and Fe 2p3/2 for CNT-LDH in Fig. S7A, S7B, S7C (ESI†) show binding energies of oxidized CNT, 2+ Ni oxidation state, and 3+ Fe oxidation state, which is consistent with those of reported NiFe LDH.[18, 25, 29] For CNT-MMO, the high resolution of C 1s spectrum shows binding energy at 283.6 eV corresponding to Ni_3C (Fig. S7D, ESI†). The Ni 2p3/2 XPS spectrum shows binding energy at 853.2 eV which is assigned to Ni0 caused by carbon reduction (Fig. S7E, ESI†).[31-33] The identification of Ni_3C and Ni^0 are consistent with the TEM results (Fig. S8A and Fig. S8B, ESI†). In addition, NiO is also identified, which is consistent with the XRD result. The XPS analysis of Fe 2p3/2 (Fig. S7F, ESI†) demonstrates that Fe is in the state of FeOOH and FeO. However, they are not detected in the XRD spectrum. We attribute this phenomenon to the ultra-small size of iron oxide or hydroxide in CNT-MMO (Fig. S9, ESI†).[34] Such small size is due to the In-grown structure, which can confine the particle growth and suppress the aggregation of MMO during calcination process.

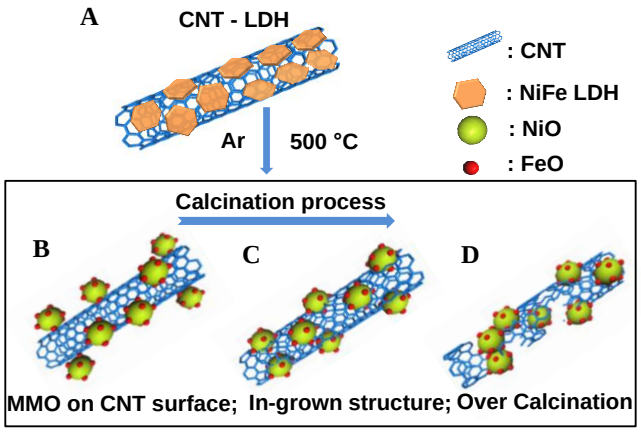

Fig. 2 Schematic drawing for: (A) structure of CNT-LDH catalyst; (B) structure of CNT-MMO-0.5 hr, where NiFe LDH are converted to MMO, but only on the surface of CNT; (C) In-grown structure of CNT-MMO catalyst, where NiO growth into CNT wall through chemical reaction with external CNT wall; and (D) structure of CNT-MMO-3 hr, where CNT structure is destroyed due to over-reaction of with NiO.

Base on the above discussion, the growth mechanism of the In-grown structure is herein proposed and illustrated in Fig. 2. It is well known that carbon can reduce the metal oxide at high temperature. Thus, when the CNT-LDH was calcined at 500 °C, the nickel oxide would be reduced at the expense of CNT wall. It is thought that the degree of reduction is a time dependent process. With 0.5 hr calcination, NiFe LDH is converted into MMO, but the resulting MMO just sticks on the surface of CNT without the formation of In-grown structure (Fig. 2B). After 2 hr calcination, MMO nanoparticles grow into CNT wall and the In-grown structure is formed (Fig. 2C). That is because the partial exhaustion of CNT wall creates the holes on CNT surface and at the same time the MMO nanoparticles partially sink into it. However, the structure of CNT will be destroyed with increased calcination time, caused by excessive exhaustion of CNT wall (Fig. 2D).

The electrochemical performance of CNT-LDH and CNT-MMO hybrid catalyst were investigated in 1 M and 0.1 M KOH solution, the results are shown in Fig. 3A. (The polarization curves for the two catalysts without iR correction are shown in Fig. S10, ESI†). In 1 M KOH solution, the CNT-MMO hybrid catalyst shows an onset potential at ~1.43 V vs. RHE, which is much lower than that of CNT-LDH catalyst (~1.48 V vs. RHE). The potential difference at current density of 10 mA/cm^2 is about 0.07 V vs. RHE. In 0.1 M KOH solution, the onset potential of OER current for CNT-MMO is also much lower than that of CNT-LDH hybrid catalyst. Comparing with CNT-MMO-0.5 hr, which is the case of physical adsorption, the CNT-MMO shows significantly improved OER activity. This result clearly demonstrates the superior of the In-grown structure. Extended calcination duration (CNT-MMO-3 hr) the OER activity is reduced due to the lower conductivity of destroyed CNT. Furthermore, the OER activity of calcined CNT, NiFe MMO, and physical mixture of calcined CNT with NiFe MMO are all not comparable to that of CNT-MMO catalyst. Comparing with the previously reported NiFe based hybrid catalysts; the In-grown NiFe MMO in CNT shows higher electrochemical performance (Table S1, ESI†).

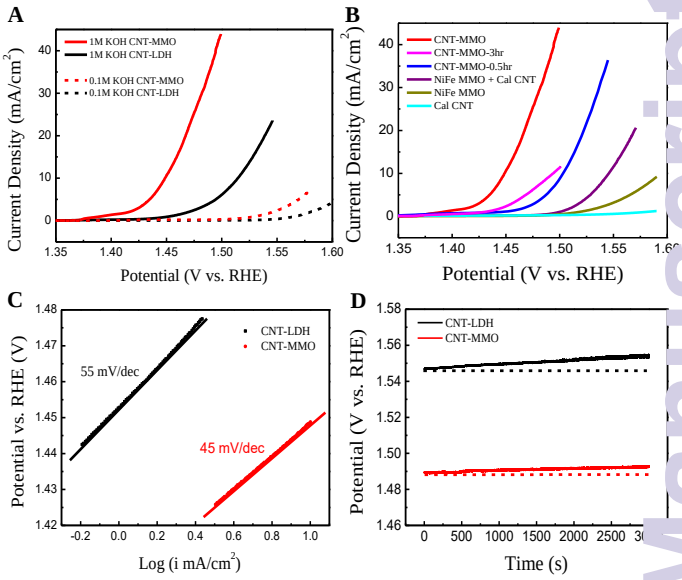

Fig. 3 (A) The iR corrected polarization curves of CNT-MMO and CNT-LDH catalyst M, 0.1 M KOH solution. The catalyst loading is 0.28 mg/cm^2; (B) The iR corrected polarization curves of CNT-MMO, CNT-MMO-3, CNT-MMO-0.5, Cal CNT, NiFe MMO and NiFe MMO + Cal CNT in 1M KOH solution; (C) The tafel plots of CNT-LDH and CNT-MMO catalysts measured in 1 M KOH solution at sweep rate of 5 mV/cm^2; (D) The stability test of CNT-LDH and CNT-MMO catalyst under 1 M KOH solution.

The tafel plots of CNT-LDH and CNT-MMO catalysts derived from the polarization curve measured in 1 M KOH are shown in Fig. 3C. The calculated tafel slope for CNT-MMO catalyst is ~45 mV/dec, which is much lower than that of CNT-LDH catalyst (~55 mV/dec). The low tafel slope directly demonstrates the excellent OER activity of CNT-MMO catalyst, contributed by In-grown structure. According to the stability test (Fig. 3D), CNT-LDH hybrid catalyst exhibits good durability under the current density of 10 mV/cm^2 (potential difference of ~9 mV at 3000s). Nevertheless, the degradation for CNT-MMO catalyst is almost negligible with potential difference of ~3 mV at 3000s. The In-grown structure could avoid the MMO nanoparticles detaching from CNT, and hence improves the durability performance.

The schematic drawing at Fig. 4 illustrates the In-grown structure and electron transfer process for OER reaction. The In-grown structure increases the interfacial area between the active catalyst (NiFe MMO) and electron conducting material (CNT), which facilitating the electron transfer from MMO nanoparticle to CNT. With efficient charge transfer process the role of CNT is significantly magnified, and the overall conductivity of the hybrid is greatly improved. Hence, the electrochemical property of this featured hybrid catalyst is extraordinarily enhanced. In addition, the increased

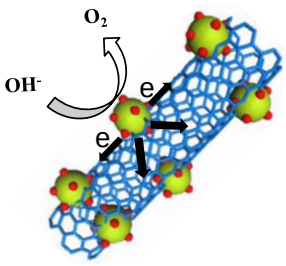

Fig. 4 Schematic drawing of OER process for CNT-MMO catalyst.

interfacial area also creates stronger interaction between MMO nanoparticle and CNT, which could stabilize the MMO in CNT.

In conclusion, a featured NiFe MMO and CNT hybrid catalyst is synthesized for OER process. The NiFe MMO catalyst is partially In-grown into CNT at the expense of CNT walls, exhibiting an unique In-grown structure. The In-grown structure is highly favorable for the charge transfer process at the interface, because of the increased interfacial area and strong interaction between NiFe MMO catalyst and CNT. The resultant hybrid catalyst demonstrates excellent OER electrocatalytic activities (onset potential of 1.43 V vs. RHE and tafel slope of ~45 mV/dec). We believe that our strategy to develop highly active MMO with CNT hybrid catalyst is applicable to prepare a library wide range of functional materials for various applications including catalysis, energy conversion and energy storage.

Notes and references

1 M. G. Walter; E. L. Warren; J. R. McKone; S. W. Boettcher; Q. Mi; E. A. Santori; N. S. Lewis, Chemical Reviews 2010, 110, 6446-6473.
2 T. R. Cook; D. K. Dogutan; S. Y. Reece; Y. Surendranath; T. S. Teets; D. G. Nocera, *Chemical Reviews* 2010, **110**, 6474-6502.
3 F. Cheng; J. Chen, *Chemical Society Reviews* 2012, **41**, 2172-2192.
4 R. M. Yadav; J. Wu; R. Kochandra; L. Ma; C. S. Tiwary; L. Ge; G. Ye; R. Vajtai; J. Lou; P. M. Ajayan, *ACS Applied Materials & Interfaces* 2015, **7**, 11991-12000.
5 H. He; L. Shi; Y. Fang; X. Li; Q. Song; L. Zhi, *Small* 2014, **10**, 4671-4676.
6 Y. Lee; J. Suntivich; K. J. May; E. E. Perry; Y. Shao-Horn, *The Journal of Physical Chemistry Letters* 2012, **3**, 399-404.
7 E. A. Paoli; F. Masini; R. Frydendal; D. Deiana; C. Schlaup; M. Malizia; T. W. Hansen; S. Horch; I. E. L. Stephens; I. Chorkendorff, *Chemical Science* 2015, **6**, 190-196.
8 R. Subbaraman; D. Tripkovic; K.-C. Chang; D. Strmcnik; A. P. Paulikas; P. Hirunsit; M. Chan; J. Greeley; V. Stamenkovic; N. M. Markovic, *Nat Mater* 2012, **11**, 550-557.
9 M. D. Merrill; R. C. Dougherty, *The Journal of Physical Chemistry C* 2008, **112**, 3655-3666.
10 C. Zhang; R. D. Fagan; R. D. L. Smith; S. A. Moore; C. P. Berlinguette; S. Trudel, *Journal of Materials Chemistry A* 2015, **3**, 756-761.
11 X. Lu; C. Zhao, *Nat Commun* 2015, **6**.
12 L.-A. Stern; X. Hu, *Faraday Discussions* 2014, **176**, 363-379.
13 F. Chekin; H. Tahermansouri; M. Besharat, *J Solid State Electrochem* 2014, **18**, 747-753.
14 M. Gao; W. Sheng; Z. Zhuang; Q. Fang; S. Gu; J. Jiang; Y. Yan, *Journal of the American Chemical Society* 2014, **136**, 7077-7084.
15 D. Friebel; M. W. Louie; M. Bajdich; K. E. Sanwald; Y. Cai; A. M. Wise; M.-J. Cheng; D. Sokaras; T.-C. Weng; R. Alonso-Mori; R. C. Davis; J. R. Bargar; J. K. Nørskov; A. Nilsson; A. T. Bell, *Journal of the American Chemical Society* 2015, **137**, 1305-1313.
16 W. D. Chemelewski; J. R. Rosenstock; C. B. Mullins, *Journal of Materials Chemistry A* 2014, **2**, 14957-14962.
17 L. Trotochaud; S. L. Young; J. K. Ranney; S. W. Boettcher, *Journal of the American Chemical Society* 2014, **136**, 6744-6753.
18 Z. Lu; W. Xu; W. Zhu; Q. Yang; X. Lei; J. Liu; Y. Li; X. Sun; X. Duan, *Chemical Communications* 2014, **50**, 6479-6482.
19 X. Long; S. Xiao; Z. Wang; X. Zheng; S. Yang, *Chemical Communications* 2015, **51**, 1120-1123.
20 M. Gong; H. Dai, *Nano Res.* 2015, **8**, 23-39.
21 M. W. Louie; A. T. Bell, *Journal of the American Chemical Society* 2013, **135**, 12329-12337.
22 X. Long; J. Li; S. Xiao; K. Yan; Z. Wang; H. Chen; S. Yang, *Angewandte Chemie International Edition* 2014, **53**, 7584-7588.
23 W. Ma; R. Z. Ma; C. X. Wang; J. B. Liang; X. H. Liu; K. C. Zhou; T. Sasaki, *Acs Nano* 2015, **9**, 1977-1984.
24 X. Yu; M. Zhang; W. Yuan; G. Shi, *Journal of Materials Chemistry A* 2015, **3**, 6921-6928.
25 M. Gong; Y. Li; H. Wang; Y. Liang; J. Z. Wu; J. Zhou; J. Wang; T. Regier; F. Wei; H. Dai, *Journal of the American Chemical Society* 2013, **135**, 8452-8455.
26 N. I. Andersen; A. Serov; P. Atanassov, *Applied Catalysis B-Environmental* 2015, **163**, 623-627.
27 D. Tang; J. Liu; X. Wu; R. Liu; X. Han; Y. Han; H. Huang; Y. Liu; Z. Kang, *ACS Applied Materials & Interfaces* 2014, **6**, 7918-7925.
28 V. Datsyuk; M. Kalyva; K. Papagelis; J. Parthenios; D. Tasis; A. Siokou; I. Kallitsis; C. Galiotis, *Carbon* 2008, **46**, 833-840.
29 J. Zhao; J. Chen; S. Xu; M. Shao; Q. Zhang; F. Wei; J. Ma; M. Wei; D. G. Evans; X. Duan, *Advanced Functional Materials* 2014, **24**, 2938-2946.
30 D. Rosenthal; M. Ruta; R. Schlögl; L. Kiwi-Minsker, *Carbon* 2010, **48**, 1835-1843.
31 J. C. de Jesús; P. Pereira; J. Carrazza; F. Zaera, *Surface Science* 1996, **369**, 217-230.
32 G. Abellan; E. Coronado; C. Marti-Gastaldo; A. Ribera; J. F. Sanchez-Royo, *Chemical Science* 2012, **3**, 1481-1485.
33 M. Gong; W. Zhou; M.-C. Tsai; J. Zhou; M. Guan; M.-C. Lin; B. Zhang; Y. Hu; D.-Y. Wang; J. Yang; S. J. Pennycook; B.-J. Hwang; H. Dai, *Nat Commun* 2014, **5**.
34 Y. N. Liang; Y. Li; C. Ang; Y. Shen; D. Chi; X. Hu, *ACS Applied Materials & Interfaces* 2014, **6**, 12406-12412.